International Forum on Aeroelasticity and Structural Dynamics
IFASD 2019
9-13 June 2019, Savannah, Georgia, USA

RANS AND DNS STUDY OF BUFFET IN SUBSONIC AND TRANSONIC FLOW

Kai M. Kruger Bastos[1] **and Earl H. Dowell**[2]

[1]Department of Mechanical Engineering and Materials Science
Duke University
Durham, NC 27708 USA
kai.bastos@duke.edu

[2]Department of Mechanical Engineering and Materials Science
Duke University
Durham, NC 27708 USA
earl.dowell@duke.edu

Keywords: Buffet, LCO, CFD

Abstract: This document explores a fluid instability known as buffet, which occurs in the subsonic, transonic and supersonic/hypersonic regimes. Buffet has been observed in experiments and various computational studies, and yet its underlying physics are not well-established. The goal of this study is to provide insight into various configurations which produce subsonic buffet and attempt to understand the flow physics at play. Both Reynolds Averaged Navier Stokes (RANS) and Direct Numerical Simulation of the Navier Stokes Equations (DNS) simulations were performed. Preliminary results for the study of transonic buffet over a range of angles of attack are also presented.

1 INTRODUCTION

A number of investigations have been made into the buffet phenomenon in both the subsonic and transonic regimes. [1–5]. These include both experimental and computational studies, with experiments going back as many as five decades [6].

The vortex shedding behavior seen in cylinders and other bluff bodies in crossflow has also been observed in stationary airfoils at high angles of attack [4, 5, 7]. These instabilities are characterized by lift, drag and moment coefficients which are periodic in time. Experimental studies have been performed over a range of angles of attack ($0^\circ < \alpha < 60^\circ$) by Tang and Dowell [4], Besem et al [5], Zhou et al [7] and Lee and Huang [8], as well as many others for various bluff bodies. This limit cycle is caused by the separation of the flow at the leading edge as the static angle of attack is increased, where the system begins to resemble a bluff body in crossflow. This vortex shedding is analogous to the von Karman vortex street [9]. According to scaling analysis of the Navier Stokes equations by Jaworski and Dowell [10], the order of magnitude estimates for the reduced frequency and the peak to peak oscillating lift in buffeting flows suggest that both quantities are of $\mathcal{O}(1)$.

Previous studies focused mainly on correct prediction of frequency in these flows, as well as prediction of the effect that wind tunnel geometry has on the shedding frequency and corrections for these wall effects. Additionally, these studies often extend to investigations of pitching

and plunging oscillating airfoils in order to determine the lock-in frequencies as a function of oscillating airfoil amplitude and for a given steady angle of attack and flow speed. These studies have not typically been concerned with prediction of mean lift coefficient ($\overline{C_L}$) or the peak-to-peak lift coefficient (ΔC_L), though one study mentions these parameters [7], or the conditions for the onset of this behavior. Figure 1 shows a typical time history of the lift coefficient for a buffeting flow for a stationary airfoil.

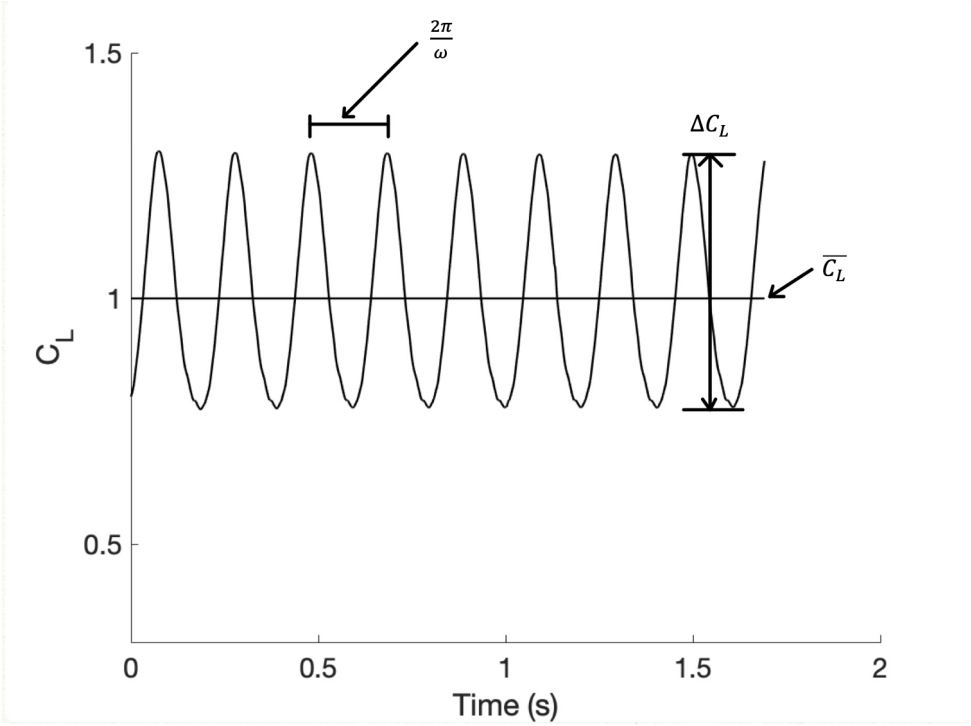

Figure 1: Typical Time History for Buffeting Flow

Transonic flow buffet dynamics are still not well understood. Exhibiting characteristics of both subsonic and supersonic flows, shockwave-boundary layer interactions (SWBLI) are a key factor. For a number of airfoil and wing, Mach number and angle of attack configurations, the flow can enter a limit cycle, creating oscillating forces on the aerodynamic bodies and creating the possibility of fatigue and therefore failure of structures. Some transonic flows exhibit a shockwave boundary layer interaction which causes the shock formed on the surface of the aerodynamic body to oscillate back and forth along its chord. Unfortunately, the physics of the transonic buffet phenomenon are not yet clear. However, it is clear that the shock causes separation downstream of the shock [1, 2, 11]. A classic experiment by McDevitt and Okuno [12] established buffet onset for the NACA0012 airfoil at transonic conditions beyond a certain angle of attack, α at a fixed Mach number. Experimental studies show that the transonic buffet phenomenon continues as α increases. Subsequently, experiments were performed on transcritical airfoils; these airfoils are designed to delay the formation of a shock on the surface of the airfoil. These, too, exhibit transonic buffet, with RANS simulations being able to capture this buffet [13, 14]. However, the simulations appear not to be able to capture the sustained buffet beyond $M = 0.8$, where experiments continued to exhibit buffeting behavior while RANS calculations predicted steady flows [2, 12]. As a phenomenon, transonic buffet is somewhat difficult to capture computationally without a particular set of parameters and turbulence models [1, 2, 14, 15]. Barakos and Drikakis [15] performed a study in which they evaluated the effectiveness of a number of turbulence models in capturing buffet over a NACA0012 profile.

There was a substantial variation in results for different turbulence models, with some turbulence models failing to produce buffet.

Buffet has been studied computationally largely in two dimensions [1, 2, 13]. This is primarily because of the fine grids and small time-steps required to capture buffet [11, 13, 14, 16], which increase the computational cost, as well as there being reasonable agreement between the 2D calculations and experimental values [2].

This paper focuses on the study of buffet over static airfoils. The subsonic case is studied with regard to its dependence on Reynolds number, and the transonic case with its dependence of angle of attack α.

2 SUBSONIC BUFFET

Low speed buffet occurs on airfoils at high angles of attack in crossflows. Buffet is characterized by large scale fluid instabilities, which manifest themselves in fluctuations in pressure on the airfoil surface. A number of studies have been performed to determine the behavior of airfoils at various angles of attack. A computational study was performed for the NACA0012, a symmetric airfoil, to determine buffet onset, capture reduced frequencies (Eqn. 1) and determine the variations in lift coefficient (Eqn. 2).

$$k = \frac{\omega c}{U_\infty} \tag{1}$$

where ω is the frequency in rad/s, c is the airfoil chord in m, and U_∞ is the freestream velocity in m/s.

$$C_L = \frac{L}{\frac{1}{2}\rho_\infty U_\infty^2 c} \tag{2}$$

where L is the lift force, perpendicular to the freestream.

A study was conducted to determine the effect of Reynolds number on the subsonic buffet phenomenon at a fixed angle of attack (α) and fixed Mach number. The unsteady Reynolds Averaged Navier Stokes equations and the Navier Stokes equations are solved discretely using ANSYS Fluent. Though not reported here, results were also obtained over a range of angle of attack, and for $30^\circ \leq \alpha \leq 60^\circ$ the results are similar.

2.1 Computational Parameters

The reference parameters for this study are as per an experiment performed by Tang and Dowell [4] and Besem et al [5], whose freestream Reynolds number was $Re = 87,000$. The experiment by Tang and Dowell [4] studied the vortex shedding phenomenon on the NACA0012 airfoil at angles of attack ($\alpha > 20^\circ$) at low Mach number ($M \approx 0.05$). This study, in conjunction with the study by Besem et al [5], which contains a correction for wind tunnel geometry, are the guiding works for the current study. Additionally, the work by Lee and Huang [8] guided the Reynolds number ranges which are studied here. Figure 1 shows a typical time history of the lift coefficient for a buffeting flow. Simulations were performed using a truncated version of the NASA grid [17] for the NACA0012 airfoil (Figs. 2 and 3) with 257 points on the airfoil in an attempt to capture low speed buffet across a range of Reynolds numbers. The NACA0012

is a 12% thick airfoil with chordwise thickness defined by a polynomial. This grid extends 20 chords in each direction as shown in Figs. 2 and 3, as the original grid's 1000-chord span was determined to be unnecessarily large for this study. The steady flow lift coefficient changes by less than 0.5% when moving from the 1000 chord span to the 40 chord span. Similarly, the reduced frequency value changes by 1% when the domain size is reduced.

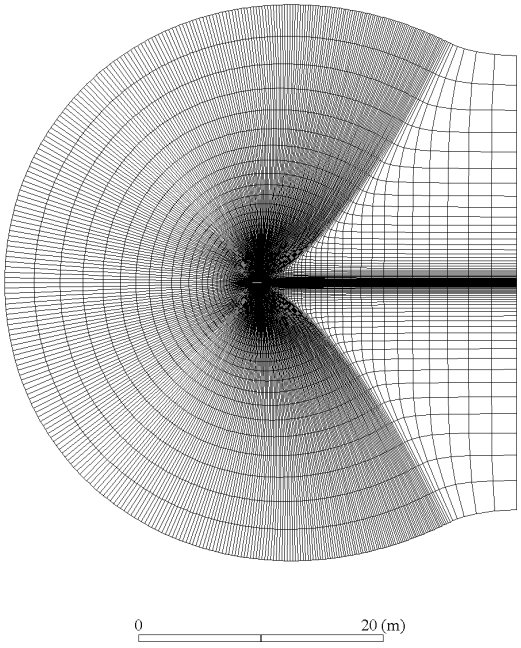

Figure 2: Truncated NASA Grid

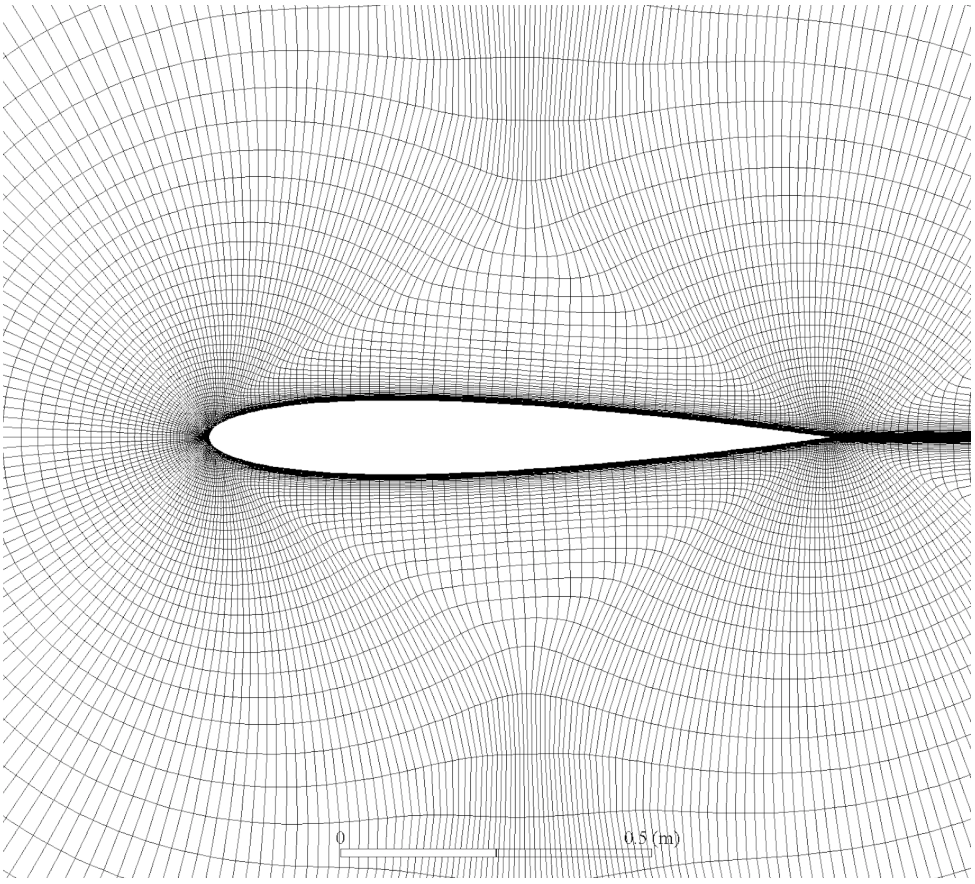

Figure 3: NASA Grid Close-Up View

2.2 Computational Model and Convergence Study

Simulations were performed using a pressure-based RANS calculation with Fluent in ANSYS 19.2. Using the coupled pressure-velocity scheme, as well as dual time-stepping, the maximum number of sub-iterations was set to 100, and the Courant number, which controls relaxation in the solution, was set to 5.

A grid convergence study was performed using four NASA grids for the NACA0012. Starting with 64 cells on the airfoil surface, each subsequent grid has twice the grid resolution. The quantities of interest in convergence are the peak-to-peak lift coefficient (ΔC_L) and the reduced frequency k. Each grid has the same span, and uses the Spalart Allmaras turbulence model, in accordance with previous studies [5, 7]. It was determined that the grid had converged when the parameters of interest were changing by less than 2% with a halving of grid spacing.

The freestream velocity is $U_\infty = 20m/s$, default values are used for turbulent model parameters and the pressure is atmospheric. To determine the dependence of the solution on turbulence model, three turbulence models were evaluated for the nominal case of $\alpha = 40^\circ$ and $Re = 87,000$: Spalart Allmaras [18], $k - \Omega\, SST$ [19] and Realizable $k - \epsilon$ [20] were evaluated for this case. It was determined that the reduced frequency and variance of lift coefficient, as well as mean lift coefficient were weakly dependent on the selected turbulence model. However, the Spalart Allmaras model [18] yielded results closest to those of Tang and Dowell [4], as well as Besem et al [5] for the nominal case of $\alpha = 40^\circ$, $Re = 87,000$.

2.3 A Sweep in Reynolds Number at $\alpha = 40°$

To determine the effect of Reynolds number on reduced frequency, a sweep was performed across a range from $Re = 50$ to $Re = 2,000,000$ using the original experimental Reynolds number of $87,000$ as a reference point, with vortex shedding appearing as in Fig. 4.

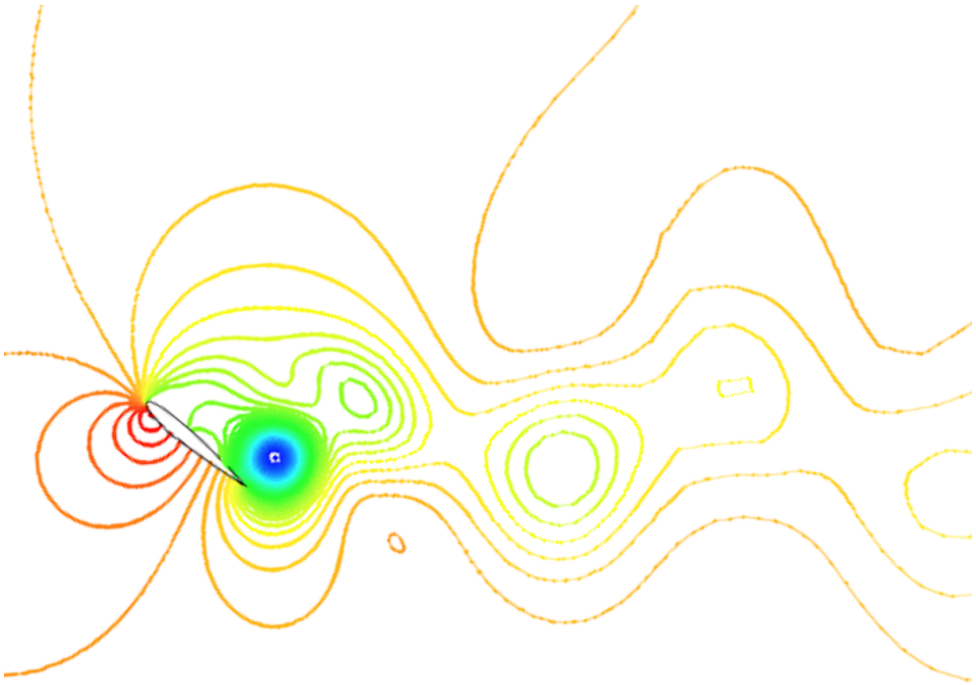

Figure 4: Instantaneous Pressure Contours for $Re = 87,000$ for $\alpha = 40°$

The time history for lift coefficient can be seen in Fig. 5, with a smooth periodic behavior, giving a dominant frequency $k = 1.009$

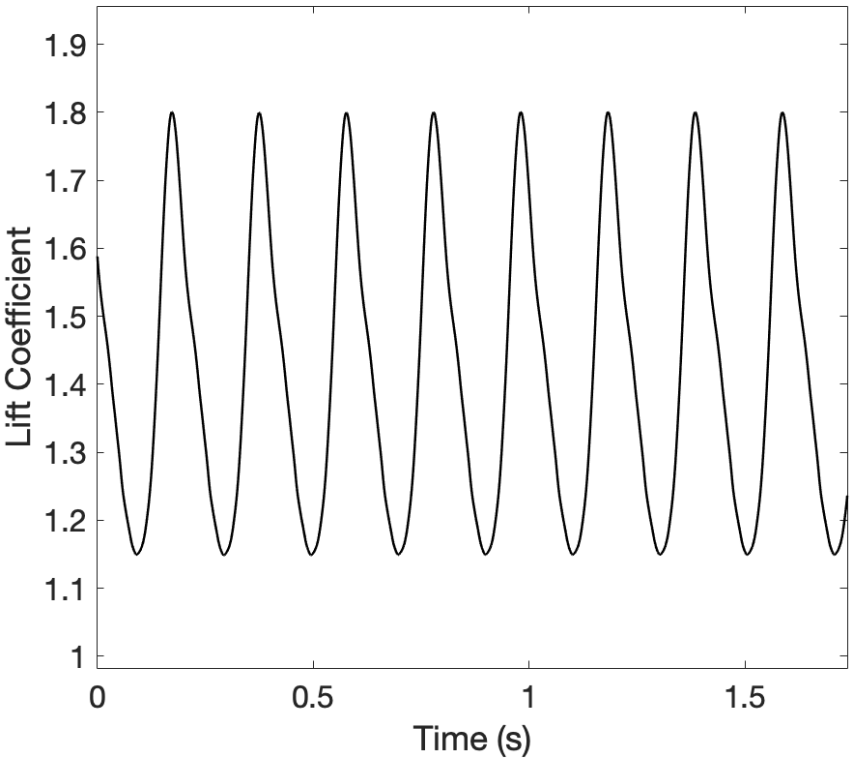

Figure 5: Lift Coefficient Time History for $Re = 87,000$

While in general this behavior is expected for bodies resembling cylinders, as seen in Fig. 6 from Blevins [21], it was expected that there would be distinct regimes of no periodicity, simple periodicity, quasi-periodicity, chaos, and then periodicity again as the Reynolds number is increased. Figures 7a, 7b show a nearly constant reduced frequency across a large range of Reynolds numbers – an unexpected behavior that was originally investigated over a smaller range of Reynolds numbers [4, 5, 8]. Lee and Huang [8] found that these flow behaviors can be categorized into laminar, subcritical, transitional and supercritical regimes based upon Reynolds number and angle of attack.

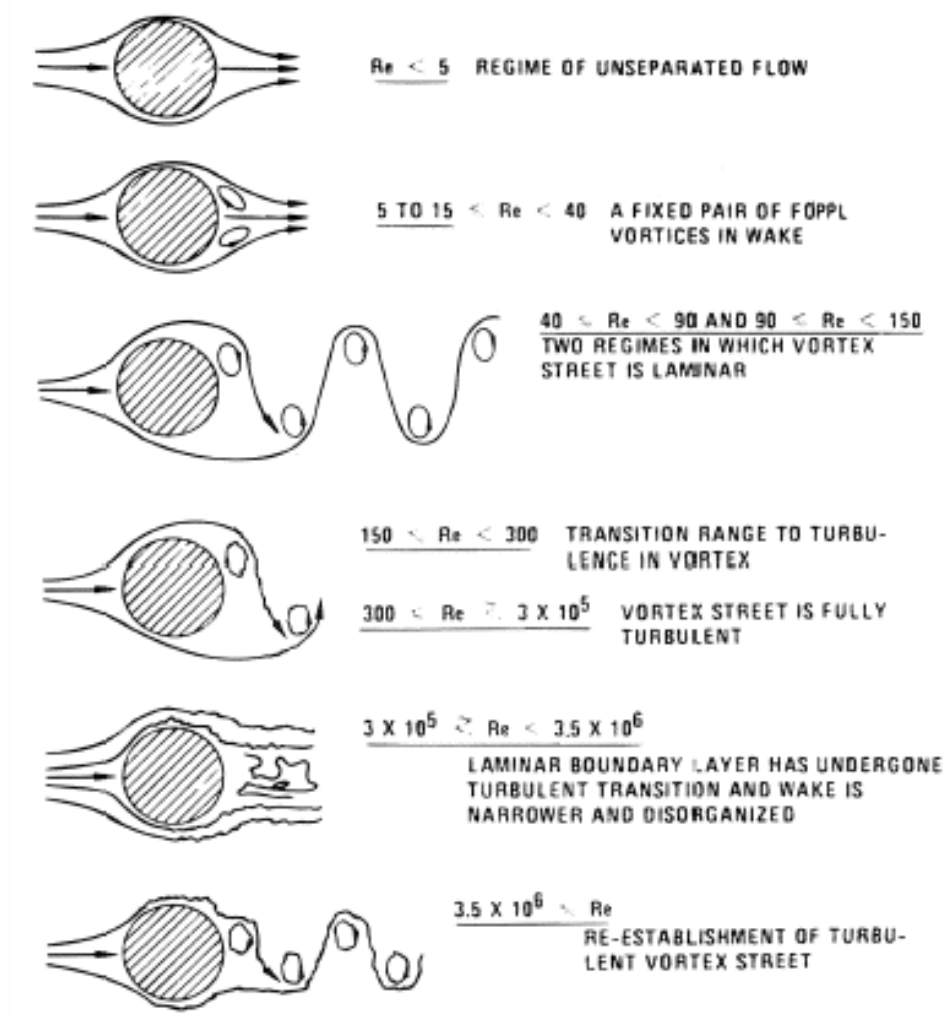

Figure 6: Flow Regimes for a Cylinder in Crossflow [21]

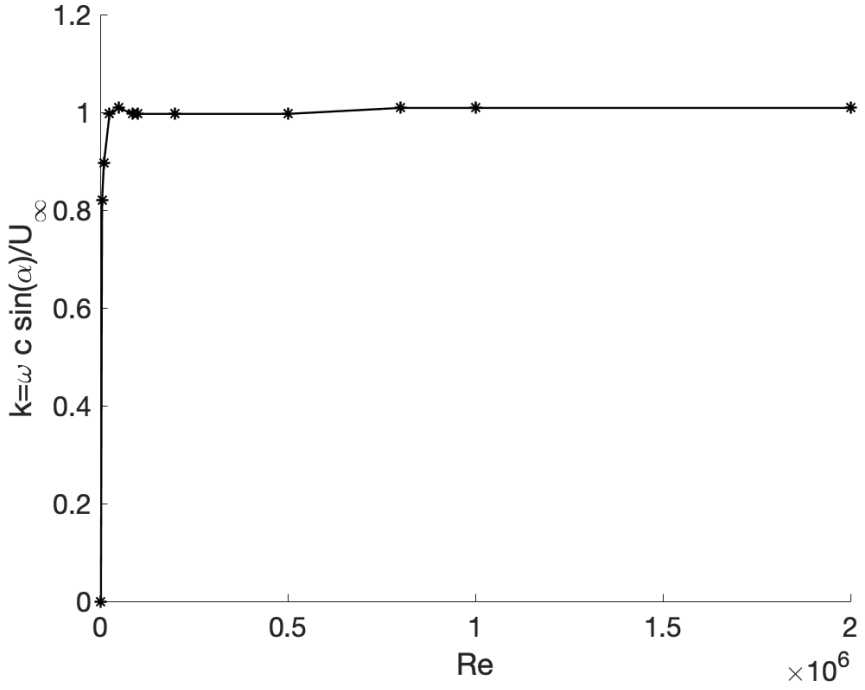

(a) $0 < Re \leq 2,000,000$

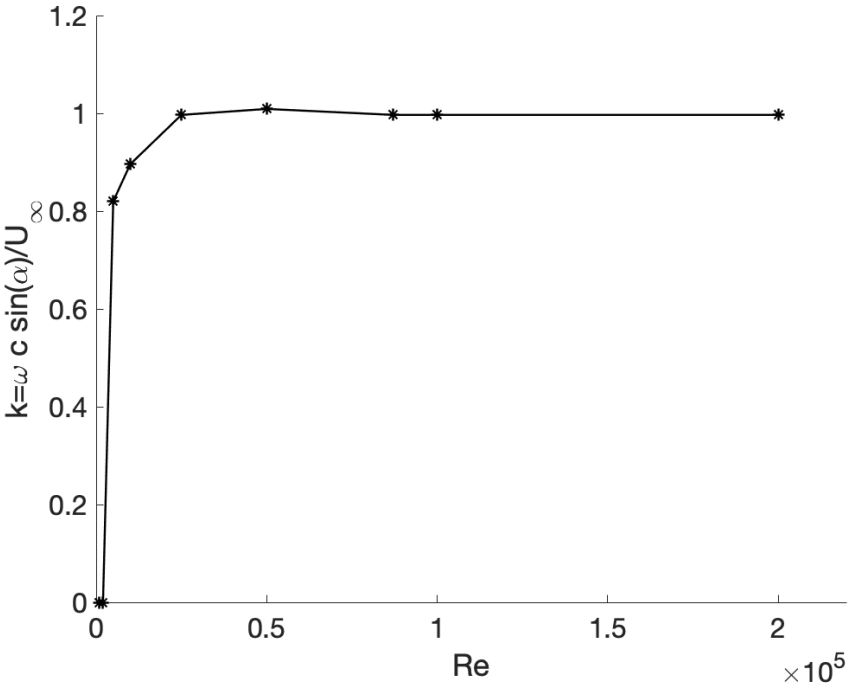

(b) $0 < Re \leq 200,000$

Figure 7: Dominant Frequency vs Reynolds Number for $\alpha = 40°$ (RANS)

The variation in time of average lift coefficient and peak to peak change (standard deviation) in lift coefficient were also determined, and these can be seen in Figs. 8a, 8b and 9a and 9b.

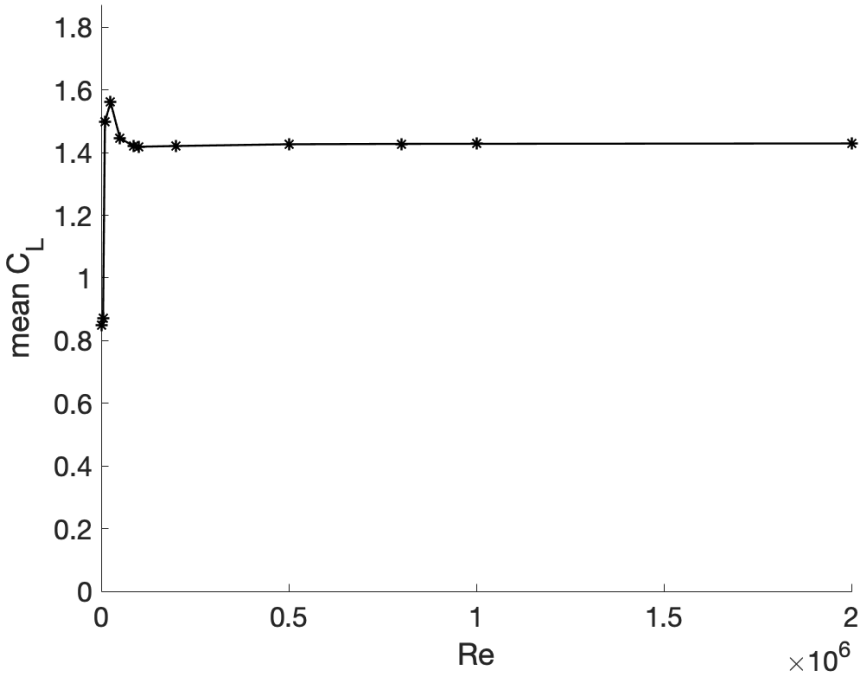

(a) $0 < Re \leq 2,000,000$

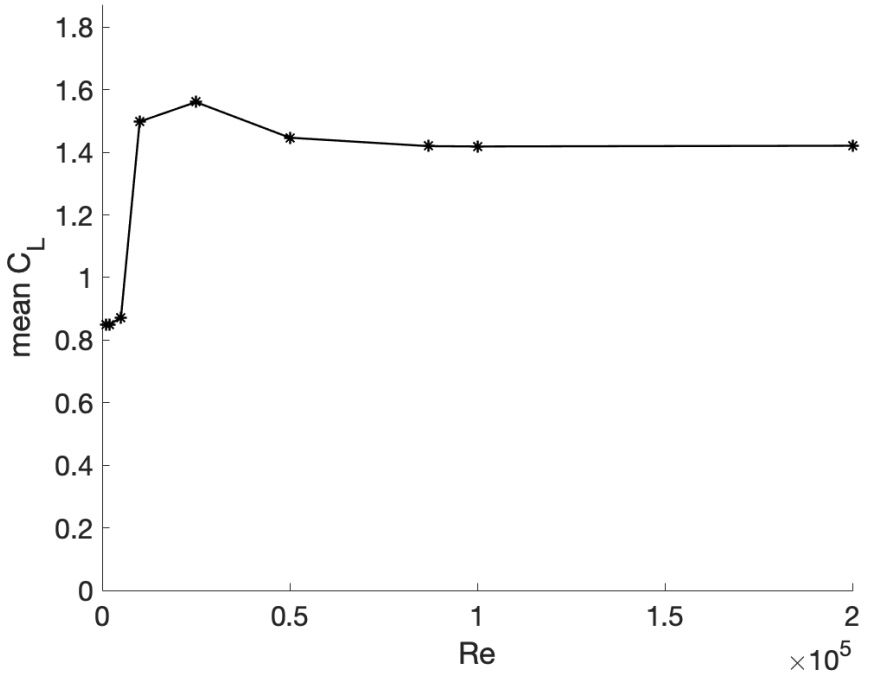

(b) $0 < Re \leq 200,000$

Figure 8: Mean C_L vs Reynolds Number for $\alpha = 40°$ (RANS)

Figure 8a shows small dependence on Reynolds number of the *mean* lift coefficient across a large range. However, there appears to be a maximum mean lift coefficient near $Re = 10^5$ and when the the Reynolds number falls below 0.2×10^4 a significant drop in mean lift coefficient

is observed.

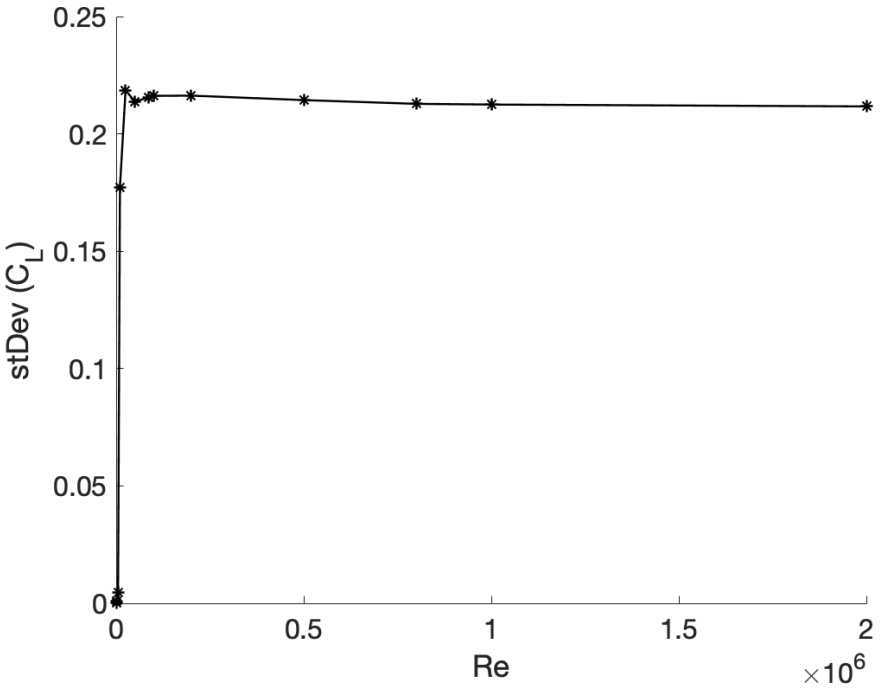

(a) $0 < Re \leq 2,000,000$

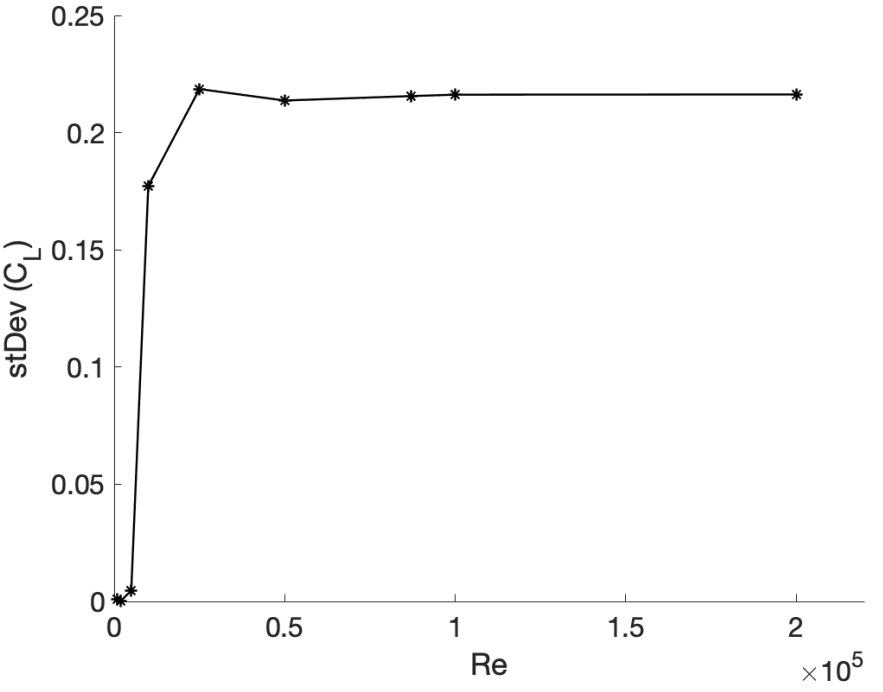

(b) $0 < Re \leq 200,000$

Figure 9: Standard Deviation of C_L vs Reynolds Number for $\alpha = 40°$ (RANS)

Similarly, the *peak-to-peak* (standard deviation) lift coefficient remains nearly constant until the Reynolds number decreases to $Re = 10^5$ and experiences the same decrease, with the lift coefficient no longer oscillating below $Re = 1500$. The transient lift coefficient at this Reynolds number, however, has a reduced frequency similar to the rest of the Reynolds range. Additionally, it is expected from the experimental results by Lee and Huang [8] that the lift coefficient remains periodic in this range, down to Reynolds numbers on the order of $Re \approx 600$.

2.4 Breakdown of Turbulence Model in RANS Simulations

As the Reynolds number decreases to $\mathcal{O}(10^3)$, lift coefficient oscillations begin to damp out using a RANS model. This is unexpected since, in the case of the cylinder in crossflow [22], vortex shedding is observed for Reynolds numbers as low as $Re \approx 47$. This result, coupled with the fact that turbulence models are generated for high Reynolds numbers (where fully resolved direct numerical simulation of the Navier Stokes equations is not feasible), suggested that there was a breakdown of the Spalart Allmaras turbulence model at sufficiently low Reynolds number.

As a result, simulations were performed using the Navier Stokes equations without a turbulence model (DNS) in an attempt to determine the onset of oscillations in lift coefficient. It was also of interest to determine where, if anywhere, the results from DNS and the RANS with Spalart Allmaras closure agree, and how large this range of Reynolds number might be.

2.5 Direct Simulations of the Navier Stokes Equations

Using the same grid, the full Navier Stokes equations were solved directly for the experimental parameters from Tang and Dowell [4]. With a Reynolds number of $Re = 87,000$, it was expected that not all of the flow features would be captured by a RANS model. However, there appears to be good agreement for reduced frequency, with the RANS and the DNS predicting reduced frequencies of $k = 1.035$ and $k = 0.936$ respectively. In fact, where the RANS solution no longer predicts flow oscillations at low Reynolds numbers, the DNS solutions continue to exhibit periodicity in lift coefficient. See the FFT shown in Fig. 10. Even at $Re \approx 800$, DNS predicts flow oscillations and a reduced frequency of $k = 1.003$.

Since the full Navier-Stokes equations are being solved rather than the RANS equations, a convergence study was performed for the DNS case using the same family of grids from NASA [17]. When the grid was determined to have converged for the parameters of interest, the same parameters were simulated for DNS cases as for the RANS cases with Spalart Allmaras turbulence model. Figures 11a and 11b show the results over a range of Reynolds numbers for both methods.

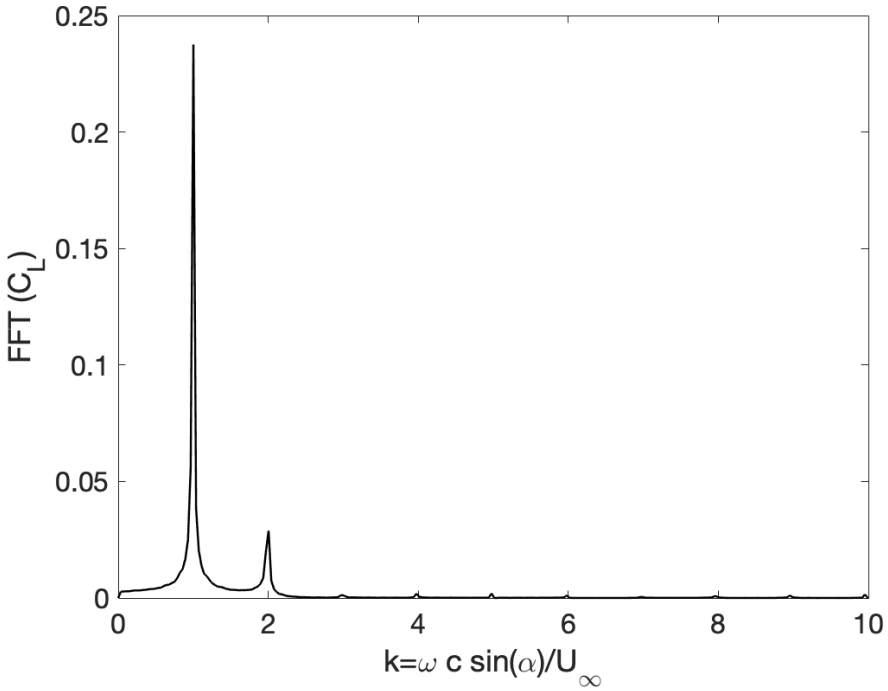

Figure 10: Frequency Spectrum for DNS at $Re = 800$

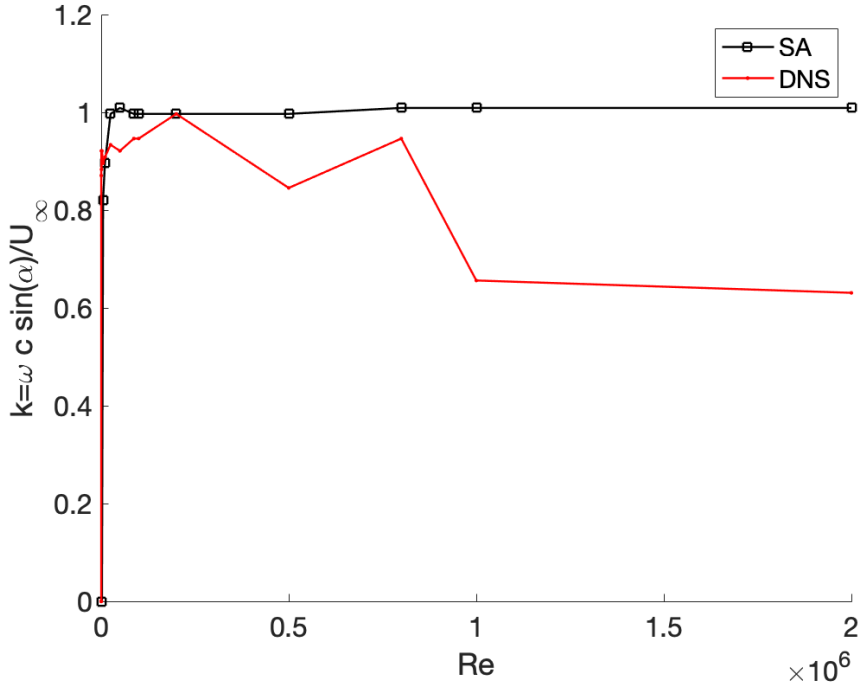

(a) $600 \leq Re \leq 2,000,000$

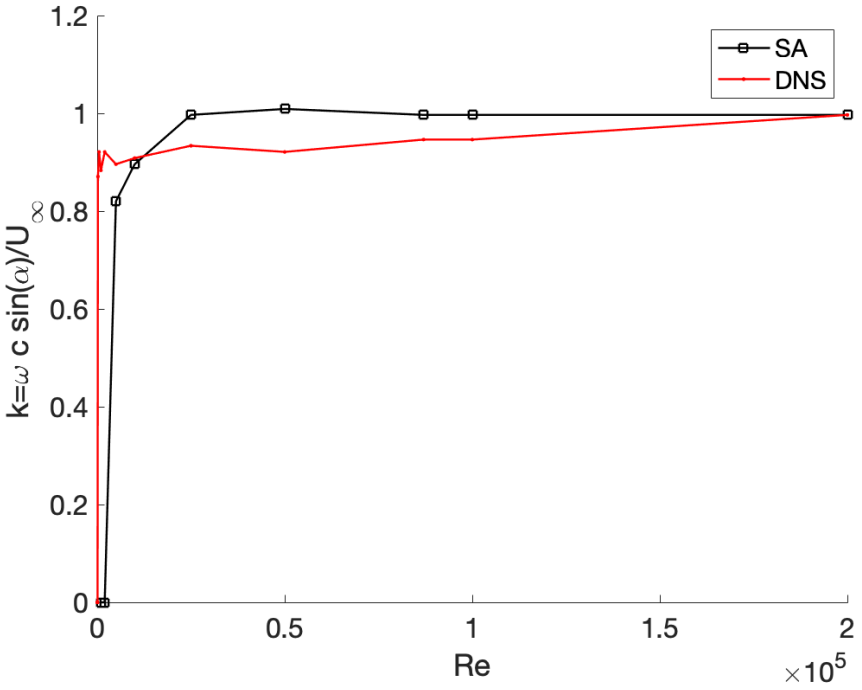

(b) $600 \leq Re \leq 200,000$

Figure 11: RANS (Spalart Allmaras) and DNS Results for Reduced Frequency Over a Range of Reynolds Numbers for $\alpha = 40°$

There is reasonably good agreement in reduced frequency over a large range, though as the Reynolds number decreases below $Re \approx 10^4$ and increases above $Re \approx 10^6$, larger discrepancies appear. There is also reasonable agreement for the mean and peak-to-peak lift coefficient, as seen in Figs. 12 and 13. The standard deviations for the oscillating lift coefficient predicted

by the RANS and DNS models differ by about a factor of 2.

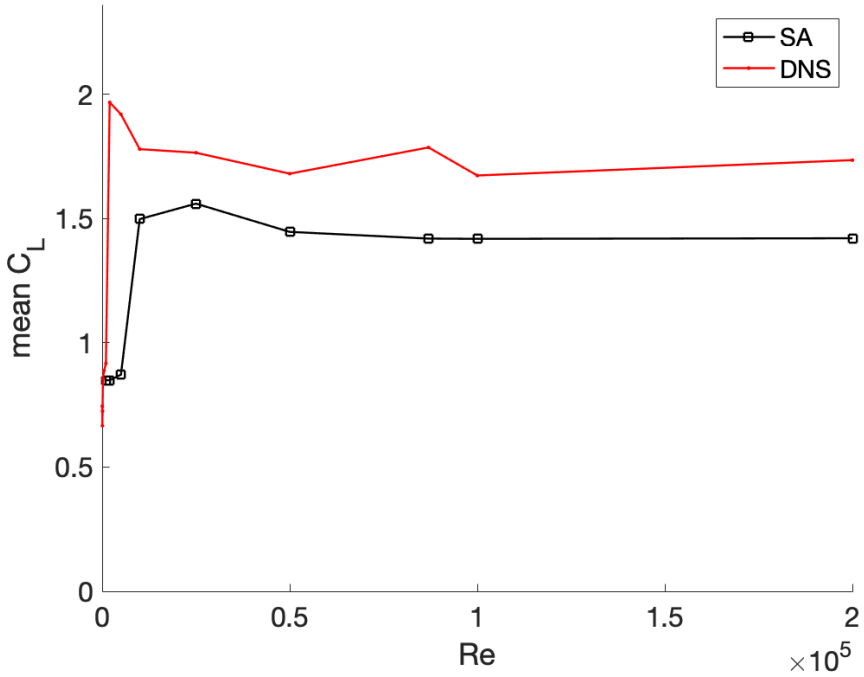

Figure 12: $\overline{C_L}$ vs Reynolds Number for Spalart Allmaras and DNS for $\alpha = 40°$

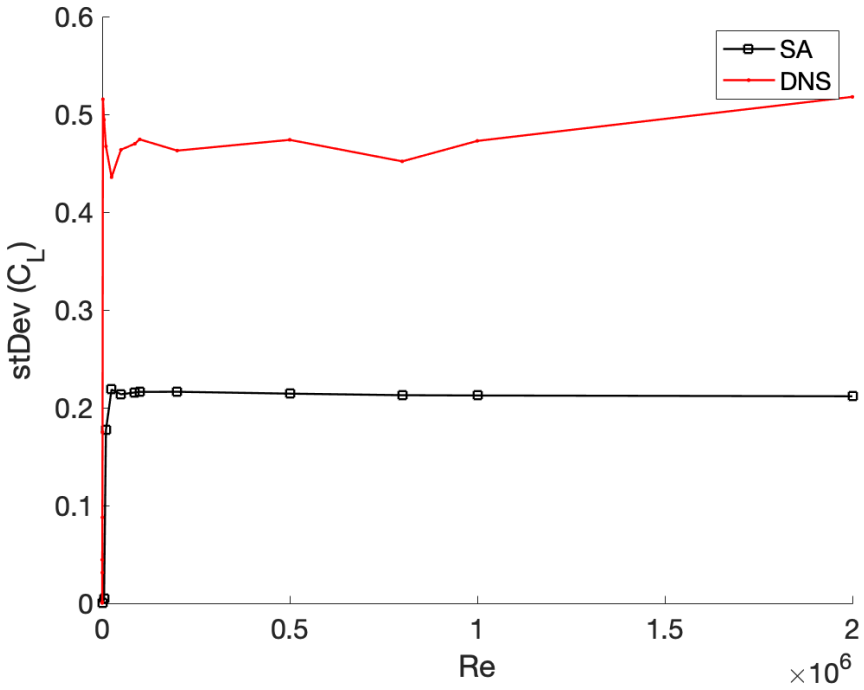

Figure 13: ΔC_L vs Reynolds Number for Spalart Allmaras and DNS for $\alpha = 40°$

As expected at the higher Reynolds numbers the frequency spectrum of the DNS simulations shows a broader spectrum while the RANS computations show a dominant frequency. See Figs. 14a and 14b for a comparison of FFTs and time histories for $Re = 87,000$. Figs. 14c and 14d compare the FFTs and time histories at a Reynolds number $Re = 1,000,000$, showing a

greater difference between the FFTs for the DNS and RANS cases.

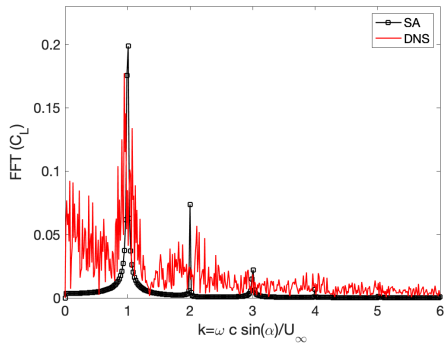

(a) FFT at $Re = 87,000$

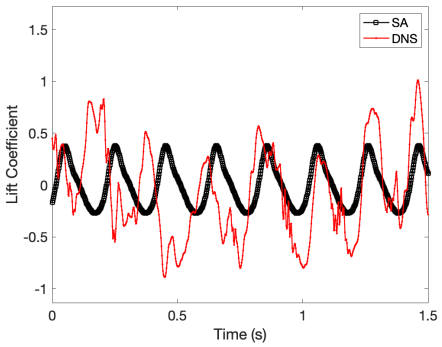

(b) Time Histories at $Re = 87,000$

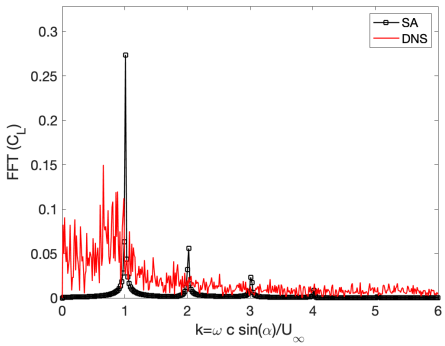

(c) FFT at $Re = 1,000,000$

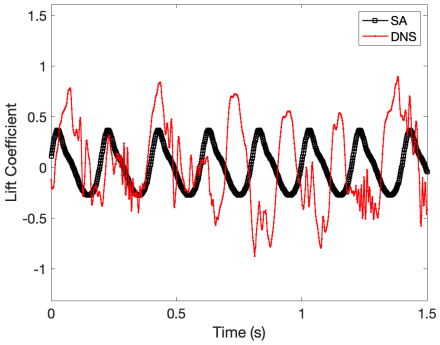

(d) Time Histories at $Re = 1,000,000$

Figure 14: FFTs and Time Histories for the RANS and DNS Cases at $\alpha = 40°$

For DNS simulations at Re as low as 100, limit cycle oscillations are still observed and the reduced frequency is of order 1 over a wide range of Re. See Fig. 15.

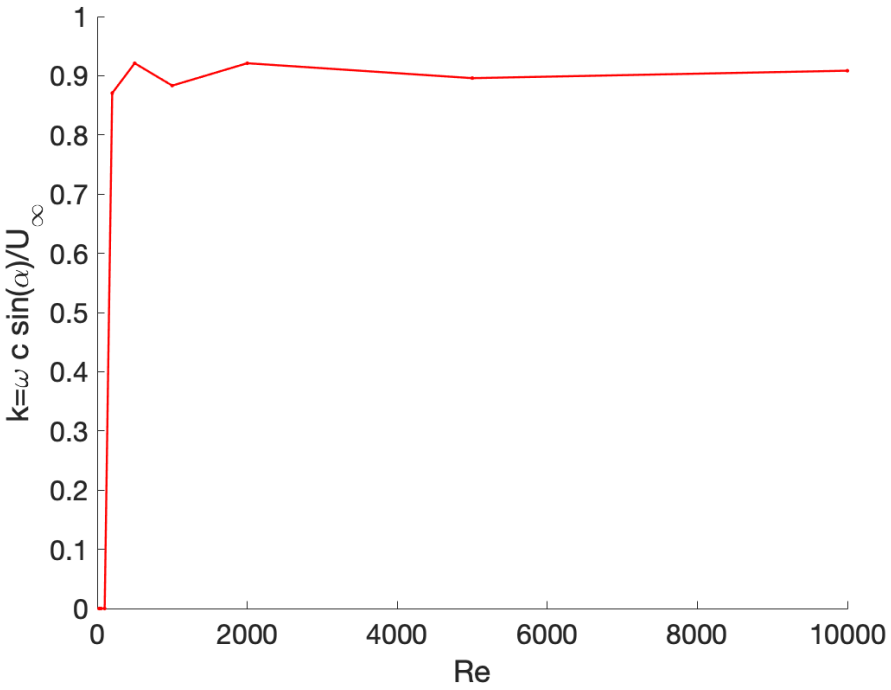

Figure 15: DNS Results for k vs Re for $Re \leq 10,000$ for $\alpha = 40^{\circ}$

2.6 Discussion of Subsonic Buffet

Given the results of these simulations, a number of observations can be made. According to the prior literature [23], a doubling in Reynolds number should lead to a halving in the size of the small scale flow structures. This would suggest that each simulation with doubled Reynolds number would require twice as fine a grid to capture surface interactions. However, the computed results show that there is weak dependence on grid resolution for large ranges of Reynolds numbers even for the DNS calculations. Given this weak dependence, it would suggest that there is small dependence on small scale structures. As such, it is argued that this separation-induced limit cycle oscillation depends mainly on large scale interactions. Of course other flow features such as drag or skin friction may depend more sensitively on smaller scales.

It is well-understood that information is lost not only when using a coarse grid, but also when performing 2D simulations. The Navier-Stokes equations exhibit vortex stretching in 3D, but not in 2D, as shown in the incompressible vorticity Eqn.(3 and 4), as vorticity cannot depend on the out-of-plane direction, so the term $\omega_j S_{ij}$ becomes zero. That is to say strain is orthogonal to vorticity. Vortex stretching is an important component of turbulent flows [23], though it seems not to have a strong effect on the ability to capture a reasonable reduced frequency for buffet in two dimensions. This may also be attributed to the fact that the experiment by Tang and Dowell [4] was performed using an airfoil which spanned the test section of the wind tunnel, allowing for quasi-two-dimensional flow characteristics.

$$\frac{D}{Dt}\omega_i = \nu\nabla^2\omega_i + \epsilon_{ijk}\nabla_j F_k \tag{3}$$

$$\frac{D}{Dt}\omega_i = \omega_j S_{ij} + \nu\nabla^2\omega_i + \epsilon_{ijk}\nabla_j F_k \tag{4}$$

where the strain tensor $S_{ij} = \nabla_j u_i$.

Given the agreement of computed results with experimental results, it can be argued that the phenomena observed by Tang and Dowell are chiefly two dimensional. This allows for far less computationally expensive simulations for predictions than if these phenomena were governed by three-dimensional interactions. Further work is suggested in the following section to determine the three-dimensional effects on vortex shedding frequency.

In the case of ΔC_L, the discrepancy between RANS and DNS is more significant. Given that the ΔC_L is more random-like in the DNS simulations, the standard deviation was used as the metric for comparison.

3 TRANSONIC BUFFET

Transonic buffet flow dynamics are not well understood. As such, a number of computational and experimental studies are being performed in order to form a more complete understanding of the physical phenomena observed in previous work.

The present work has focused on the study of transonic buffeting flow after the work of Raveh [11], Raveh & Dowell [24], Giannelis [1]. Simulations were performed in Fluent using a truncated version of the NASA grid [17] for the NACA0012 airfoil with 257 points on the airfoil in an attempt to capture transonic buffet. This grid extends 40 chords in each direction. This grid

was determined to have converged for the reduced frequency, but not for the peak-to-peak lift coefficient. The computational model for this case was as per the paper by Vio and Giannelis on the effect of angle of attack and Mach number on transonic buffet [14], and is outlined as follows:

> "Discretisation of the steady RANS equations is performed with Roes scheme, using the third-order scheme for the inviscid fluxes and second-order central differencing for the viscous and thermal fluxes. A first-order upwind scheme is used for the turbulent convective quantities. Interpolation of the state vector and cell coefficient matrix is performed through a blended third-order upwind/fourth-order central difference scheme, to reduce the numerical dissipation induced by the upwind differencing"

3.1 Computational Model Parameters

As per Giannelis and Vio [1], simulations were attempted using a density-based RANS calculation with Fluent in ANSYS 19.2, using the Spalart Allmaras [18] turbulence model. The maximum number of sub-iterations was set to 100, and the Courant number was set to 5.

3.2 An Angle of Attack Sweep at $M_\infty = 0.72$

Simulations were performed for angles of attack below the buffet boundary, and the angle of attack was increased until buffet offset was observed. The angles simulated for this set of parameters were $3.5° \leq \alpha \leq 8°$. The Reynolds numbers for these flows were $Re = 10,000,000$.

3.3 Transonic Buffet Results

Buffet onset was expected to occur near $\alpha = 4°$ based on computations performed by Crouch et al [2]. As expected, buffet was not observed at $\alpha = 3.5$, but had clearly appeared at $\alpha = 4.5°$ and continued to buffet up to $\alpha = 7°$. See Fig. 16 for the reduced frequency plotted vs angle of attack. The reduced frequency was expected to be nearly constant, however these results exhibit an increasing frequency with increasing α, up to buffet offset at $\alpha = 7°$. The transient reduced frequency is also reported on Fig. 16, though this damps out after about twenty cycles. For the cases at $\alpha = 3.5°$ and $\alpha = 8°$, the transient solution was too heavily damped to extract a meaningful frequency. Whether the variation in k over the range of angles is a function of of grid resolution is currently being investigated.

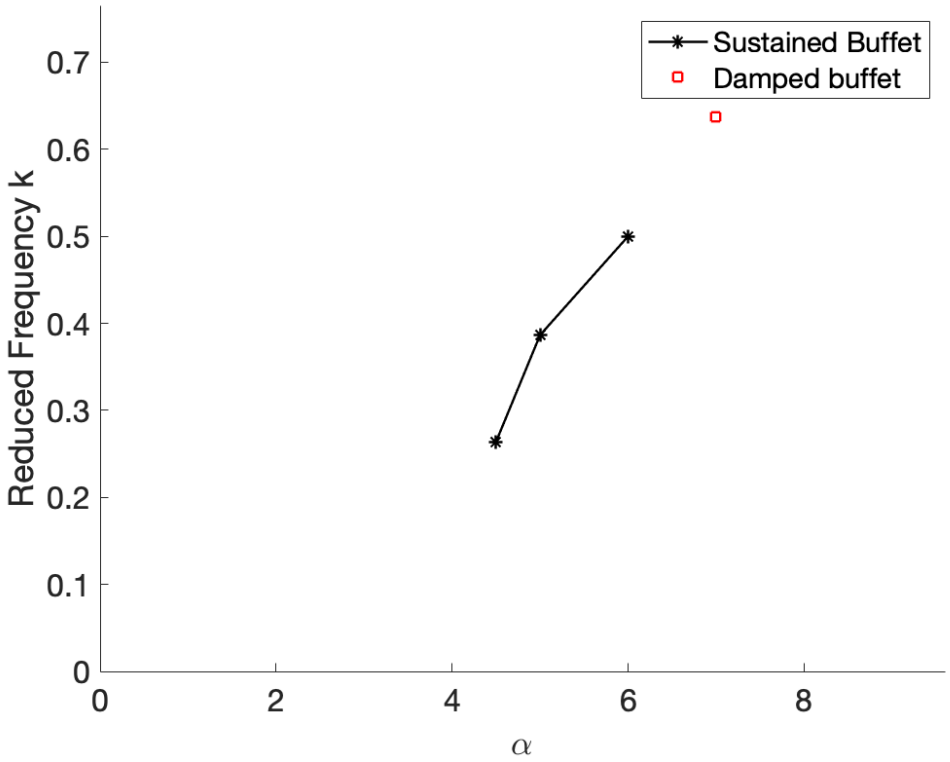

Figure 16: k vs α for $M_\infty = 0.72$, $Re = 10,000,000$

The peak-to-peak lift coefficient varies over the range of α, as shown in Fig. 17.

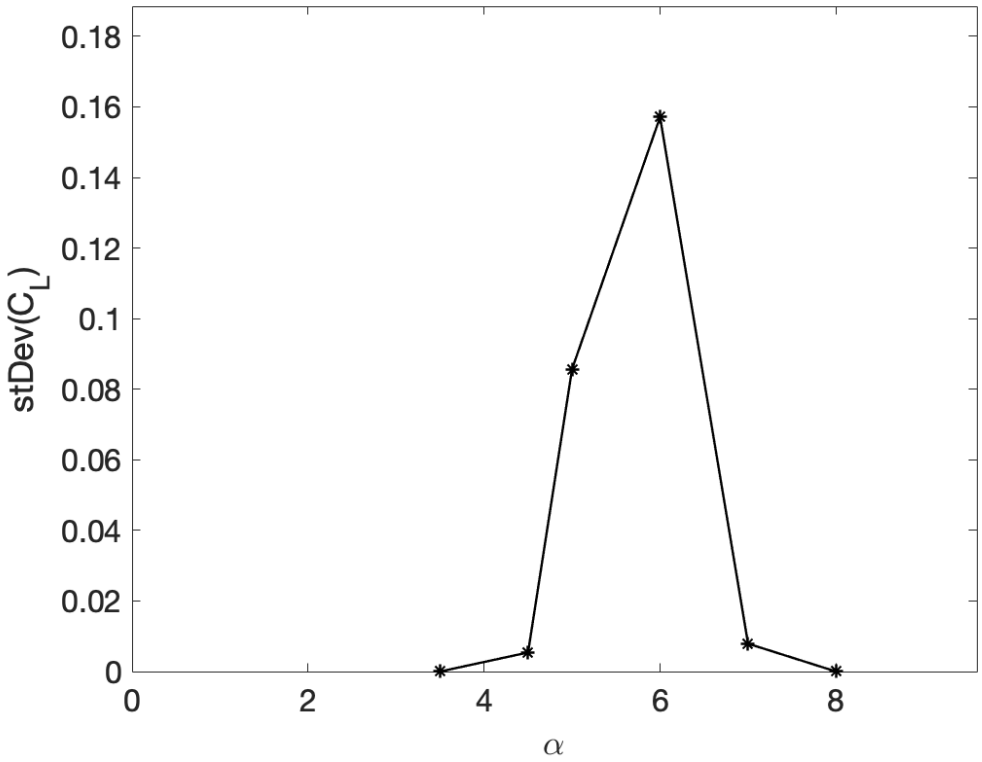

Figure 17: Standard Deviation of C_L vs α for $M_\infty = 0.72$, $Re = 10,000,000$

Though these values may not be fully converged, this is a first approximation for the qualitative behavior of peak-to-peak lift coefficient in this range. It is expected that there will be a maximum ΔC_L in this range, at which the limit cycle has its greatest amplitude.

3.4 Discussion of Transonic Buffet

The results of these preliminary simulations are promising. Buffet with converged reduced frequency is produced with grid spacing far larger than the $\mathcal{O}\ (0.15\%)$ of the chord recommended by Crouch [2]. However, it is possible that it is necessary to meet this requirement in order to converge in buffet lift amplitude as distinct from reduced frequency. Nevertheless, it is possible to make observations based on these early results.

Current results show buffet onset at the expected combination angle of attack, Mach number and Reynolds number. Additionally, the reduced frequency is of $\mathcal{O}(1)$, as expected from the scaling analysis by Jaworski and Dowell [10]. These results show a maximum for reduced frequency and buffet amplitude, though they occur at different angles of attack. A doubling in grid resolution results in an $\mathcal{O}(2)$ reduction in buffet oscillating lift coefficient amplitude; the reduced frequency appears to depend weakly on grid resolution. Further work will be performed to compare buffet amplitudes to the work of Goncalves and Houdeville [25]

Buffet is heavily dependent on turbulence closure when using RANS [15], and work will continue to determine the ability to capture buffet using not only various turbulence models, but also the full Navier Stokes Equations.

The feasibility of performing 3D transonic buffet calculations is determined mainly by computing resources and time. While it is desirable to study these phenomena in three dimensions, the focus will remain on 2D buffet for the time being.

4 PRINCIPAL OBSERVATIONS, CONCLUSIONS AND FUTURE WORK

4.1 Subsonic Flow Observations and Conclusions

Using RANS simulations, it is found that the reduced frequency and oscillating lift coefficient on a NACA 0012 airfoil at high angle of attack are insensitive to Reynolds number over a wide range of Reynolds number. DNS models are feasible for buffeting subsonic flow and the DNS and RANS results agree reasonably well for reduced frequency over a wide range of Reynolds number. The standard deviations of the lift oscillations show insensitivity to Reynolds number over a wide range, but with a difference between the two CFD models of about a factor of 2. The DNS and RANS solution do differ more in the low Reynolds number range, i.e. $Re < 10,000$ as expected.

In the subsonic case, the work of Zhou et al [7] allows for a starting point to determining the effects of the wind tunnel walls on the experimental results obtained by Tang and Dowell [4]. A 3D model of this experimental case is being prepared for simulations to determine the effect of the spanwise dimension on the parameters of interest. This will allow for the study of three-dimensional vortex structures being shed from the airfoil in the tunnel.

4.2 Transonic Flow Observations and Conclusions

RANS simulation results for reduced frequency and oscillating lift are similar to those found by previous investigators.

4.3 Future Work

One of the issues with all buffet wind tunnel studies is the possible effect of the wind tunnel walls. See, for example, the work of Fanny Besem et al [5] and Tong Zhou et al [7] on the effect of the wind tunnel wall in the Tang and Dowell [4] subsonic experiment. Extension of their work to possible three-dimensional effects is planned. Also two dimensional work on the transonic experiment of McDevitt and Okuno [12] is planned.

Another important topic for future work is to extend DNS studies to the transonic case. In the that regard it is well to remember that grid convergence for the DNS simulations must be established; it is expected that the DNS simulations will be more computationally costly than RANS studies and transonic cases are already ten times more computationally costly than subsonic cases. Finally, three dimensional buffet over wings will be studied as greater computational resources become available to follow the work of Iovnovich and Raveh [13].

5 REFERENCES

[1] Giannelis, N. F., Vio, G. A., and Levinski, O. (2017). A review of recent developments in the understanding of transonic shock buffet. *Progress in Aerospace Sciences*, 92, 3984. doi:10.1016/j.paerosci.2017.05.004.

[2] Crouch, J., Garbaruk, A., and Magidov, D. (2007). Predicting the onset of flow unsteadiness based on global instability. *Journal of Computational Physics*, 224(2), 924940. doi: 10.1016/j.jcp.2006.10.035.

[3] Gibb, J. (1988). *The Cause and Cure of Periodic Flows at Transonic Speed*. Ph.D. thesis, Cranfield University.

[4] Tang, D. and Dowell, E. H. (2014). Experimental aerodynamic response for an oscillating airfoil in buffeting flow. *AIAA Journal*, 52(6), 11701179. doi:10.2514/1.j052077.

[5] Besem, F. M., Kamrass, J. D., Thomas, J. P., et al. (2016). Vortex-induced vibration and frequency lock-in of an airfoil at high angles of attack. *Journal of Fluids Engineering*, 138(1), 011204.

[6] Hilton, W. F. and Fowler, R. (1952). *Photographs of shock wave movement*. HM Stationery Office.

[7] Zhou, T., Feng, S.-S., and Dowell, E. H. (2018). Buffeting and lock in of an airfoil at high angle of attack. *Journal of Aircraft*, 55(2), 771780. doi:10.2514/1.c034432.

[8] Lee, H.-W. and Huang, R.-F. (1998). Frequency selection of wake flow behind a NACA0012 wing. *Journal of Marine Science and Technology*, 6(1), 29–37.

[9] Von Karman, T. (1912). Uber den mechanismus des flussigkeits-und luftwiderstandes. *Phys. Z.*, 49–59.

[10] Jaworski, J. W. and Dowell, E. H. (2012). Scaling analysis for aeroelastic phenomena using the Navier-Stokes fluid model. *AIAA Journal*, 50(11), 2622–2626.

[11] Raveh, D. E. (2009). Numerical study of an oscillating airfoil in transonic buffeting flows. *AIAA Journal*, 47(3), 505515. doi:10.2514/1.35237.

[12] McDevitt, J. and Okuno, A. (1985). Static and dynamic pressure measurements on a NACA 0012 airfoil in the ames high Reynolds number facility. NASA TP-2485. *National Aeronautics and Space Administration*.

[13] Iovnovich, M. and Raveh, D. E. (2012). Reynolds-averaged Navier-Stokes study of the shock-buffet instability mechanism. *AIAA Journal*, 50(4), 880890. doi:10.2514/1.j051329.

[14] Giannelis, N. F., Levinski, O., and Vio, G. A. (2018). Influence of Mach number and angle of attack on the two-dimensional transonic buffet phenomenon. *Aerospace Science and Technology*, 78, 89101. doi:10.1016/j.ast.2018.03.045.

[15] Barakos, G. and Drikakis, D. (2000). Numerical simulation of transonic buffet flows using various turbulence closures. *International Journal of Heat and Fluid Flow*, 21(5), 620–626.

[16] Rumsey, C. L., Sanetrik, M. D., Biedron, R. T., et al. (1996). Efficiency and accuracy of time-accurate turbulent Navier-Stokes computations. *Computers & Fluids*, 25(2), 217–236.

[17] Rumsey, C., Smith, B., and Huang, G. (2010). Description of a website resource for turbulence modeling verification and validation. In *40th Fluid Dynamics Conference and Exhibit*. p. 4742.

[18] Spalart, P. and Allmaras, S. (1992). A one-equation turbulence model for aerodynamic flows. In *30th Aerospace Sciences Meeting and Exhibit*. p. 439. doi:10.2514/6.1992-439.

[19] Menter, F. R. (2009). Review of the shear-stress transport turbulence model experience from an industrial perspective. *International Journal of Computational Fluid Dynamics*, 23(4), 305316. doi:10.1080/10618560902773387.

[20] Shih, T.-H., Liou, W. W., Shabbir, A., et al. (1995). A new k- eddy viscosity model for high Reynolds number turbulent flows. *Computers & Fluids*, 24(3), 227238. doi:10.1016/0045-7930(94)00032-t.

[21] Blevins, R. D. (1977). Flow-induced vibration. *New York, Van Nostrand Reinhold Co., 1977. 377 p.*

[22] Williamson, C. H. (1996). Vortex dynamics in the cylinder wake. *Annual Review of Fluid Mechanics*, 28(1), 477–539.

[23] Pope, S. B. (2000). *Turbulent flows*. Cambridge University Press.

[24] Raveh, D. and Dowell, E. (2011). Frequency lock-in phenomenon for oscillating airfoils in buffeting flows. *Journal of Fluids and Structures*, 27(1), 89–104.

[25] Goncalves, E. and Houdeville, R. (2004). Turbulence model and numerical scheme assessment for buffet computations. *International Journal for Numerical Methods in Fluids*, 46(11), 1127–1152.

COPYRIGHT STATEMENT